Medicine Meets Virtual Reality 18
J.D. Westwood et al. (Eds.)
IOS Press, 2011

doi:10.3233/978-1-60750-706-2-623

High-Field MRI-Compatible Needle Placement Robot for Prostate Interventions

Hao SU[a,1], Alex CAMILO[a], Gregory A. COLE[a], Nobuhiko HATA[b]
Clare M. TEMPANY[b] and Gregory S. FISCHER[a]
[a]*Worcester Polytechnic Institute, Worcester, MA*
[b]*Brigham and Women's Hospital, Harvard Medical School, Boston, MA*

Abstract. This paper presents the design of a magnetic resonance imaging (MRI) compatible needle placement system actuated by piezoelectric actuators for prostate brachytherapy and biopsy. An MRI-compatible modular 3 degree-of-freedom (DOF) needle driver module coupled with a 3-DOF *x-y-z* stage is proposed as a slave robot to precisely deliver radioactive brachytherapy seeds under interactive MRI guidance. The needle driver module provides for needle cannula rotation, needle insertion and cannula retraction to enable the brachytherapy procedure with the preloaded needles. The device mimics the manual physician gesture by two point grasping (hub and base) and provides direct force measurement of needle insertion force by fiber optic force sensors. The fabricated prototype is presented and an experiment with phantom trials in 3T MRI is analyzed to demonstrate the system compatibility.

Keywords. MRI compatible robot, prostate brachytherapy, biopsy.

1. Introduction

Prostate cancer continues to be the most common male cancer and the second most common type of cancer in human. The estimated new prostate cancer cases (192,280) in 2009 account for 25% incident cases in men [1]. The current "gold standard" transrectal ultrasound (TRUS) for guiding both biopsy and brachytherapy is accredited for its real-time nature, low cost, and ease of use. However, TRUS-guided biopsy has a detection rate as low as 20%-30% and the radiation seeds cannot be effectively observed on the images [2]. On the other hand, the MRI-based medical diagnosis paradigm capitalizes on the novel benefits and capabilities of the scanner. These are created by the combination of capability for detecting seeds, high-fidelity soft tissue contrast and spatial resolution. The challenges, however, arise from the manifestation of the bidirectional MRI compatibility requirement - both the device should not disturb the scanner function and should not create image artifacts and the scanner should not disturb the device functionality. Moreover, the confined physical space in closed-bore high-field MRI presents formidable challenges for material selection and mechanical design. Early MRI-compatible robots focus on manual driven or ultrasonic motor driven and the latter cannot run during imaging due to significant signal loss. Chinzei,

[1] Corresponding Author. Hao Su, Automation and Interventional Medicine (AIM) Robotics Laboratory, Worcester Polytechnic Institute, Higgins Lab 130, 100 Institute Road, Worcester, MA 01609, USA. Tel.: +1-508-831-5191; Fax: +1-508-831-5680; E-mail: haosu@wpi.edu.

et al. developed a general-purpose robotic assistant for open MRI [3] that was subsequently adapted for transperineal intraprostatic needle placement. Krieger et al. [4] presented a 2-DOF passive, un-encoded, and manually manipulated mechanical linkage to aim a needle guide for transrectal prostate biopsy with MRI guidance. Stoianovici et al. [5] described a MRI-compatible pneumatic stepper motor PneuStep, which has a very low level of image interference. Song et al. [6] presented a pneumatic robot for MRI-guided transperineal prostate biopsy and brachytherapy. However the scalability, simplicity, size and inherent robustness of electromechanical systems present a clear advantage over pneumatically actuated systems [7-9]. The difficulty arises from the actuator driving controller that usually induces significant image artifact using off-the-shelf control circuits [10-11].

Needle steering is becoming a practical technique to address needle placement accuracy issues in recent years. Mahvash et al. [12] have experimentally demonstrated that increased needle velocity is able to minimize tissue deformation and damage and reduce position error. To bridge the gap between MRI compatible mechatronics and needle steering techniques, the contributions of this paper are: (1) design of a modular needle driver that can be coupled to a base Cartesian motion platform to improve feasibility and accuracy of MRI-guided prostate interventions and their outcome and (2) experimental demonstration of real-time *in-situ* MRI compatibility and potential for multiple imager compatible surgery. *To the authors' knowledge, this is the first needle steering robot capable of operating in real-time MRI.*

2. Methods and Materials

In this paper, we presented a 3-DOF needle driver as slave robot to provide haptic feedback as shown in Fig. 1. The overall goal is to provide force feedback using fiber optic force sensor during interventional MRI-guided prostate interventions [13-14]. The primary design requirements and the features of the needle driver include:

1) *3-DOF motion needle driver.* It provides cannula rotation and insertion (2-DOF) and stylet translation (1-DOF). The independent rotation and translation motion of the cannula can increase the targeting accuracy while minimize the tissue deformation and damage.
2) *Safety.* Interventional robots require a redundant safety mechanism. Three approaches are implemented to minimize the consequences of system malfunction. a) Mechanical travel limitations mounted on the needle insertion axis that prevents linear motor rod running out of traveling range; b) Software calculates robot kinematics and watchdog routine that monitors robot motion and needle tip position; and c) Emergency power button that can be triggered by the operator.
3) *MRI Compatibility.* The robot components are primarily constructed of acrylonitrile butadiene styrene (ABS) and acrylic. Ferromagnetic materials are avoided. Limiting the amount of conductive hardware ensures imaging compatibility in the mechanical level. The piezoelectric driver has proven minimal image interference in the electrical level.
4) *Operation in confined space.* To fit into the scanner bore, the width of the driver is limited to 6*cm* and the operational space when connected to a base platform is able to cover the perineal area using traditional brachytherapy 60 *mm* × 60*mm* templates.

5) *Sterilization*. Only the needle clamp and guide (made of low cost plastic) have contact with the needle and are disposable.
6) Compliance with transperineal needle placement, as typically performed during a TRUS guided implant procedure. This design aims to place the patient in the supine position with the legs spread and raised with similar configuration to that of TRUS-guided brachytherapy.

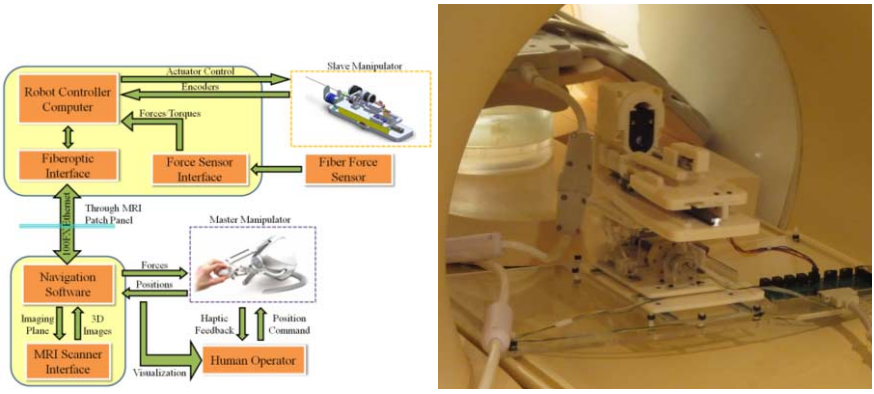

Figure 1: (Left) System architecture for the master - slave haptic interface. The fiber optic force sensor and robot are placed near the iso-center of the MRI scanner, the master manipulator is connected to the navigation software interface, and the two are couple through the robot controller in the scanner room using a fiber optic network connection. (right) The robot prototype in the bore of a 3T MRI scanner with a phantom.

2.1. Needle Placement Robot Design

The needle placement robot consists of a needle driver module (3-DOF) and Cartesian positioning module (3-DOF). The material is rapid prototyped with ABS and laser cut acrylic. Considering the supine configuration and the robot workspace, the width of the robot is limited to 6*cm*. As shown in Fig. 2 (left), the lower layer of the needle driver module is driven with linear piezoelectric motor and the upper layer provides cannula rotation motion and stylet prismatic motion.

To design a needle driver that allows a large variety of standard needles, a new clamping device shown in Fig. 2 (right) rigidly connects the needle shaft to the driving motor mechanism. This structure is a collet mechanism and a hollow screw made of stereolithography ABS is twisted to fasten the collet thus rigidly locks the needle shaft on the clamping device. The clamping device is connected to the rotary motor through a timing belt that can be fastened by an eccentric belt tensioner. The clamping device is generic in the sense that we have designed 3 sets of collets and each collet can accommodate a width range of needle diameters. The needle driver is designed to operate with standard MR-compatible needles of various sizes. The overall needle diameter range is from 25 *Gauge* to 7 *Gauge*. By this token, it can not only fasten brachytherapy needle, but also biopsy needles and most other standard needles instead of designing some specific structure to hold the needle handle.

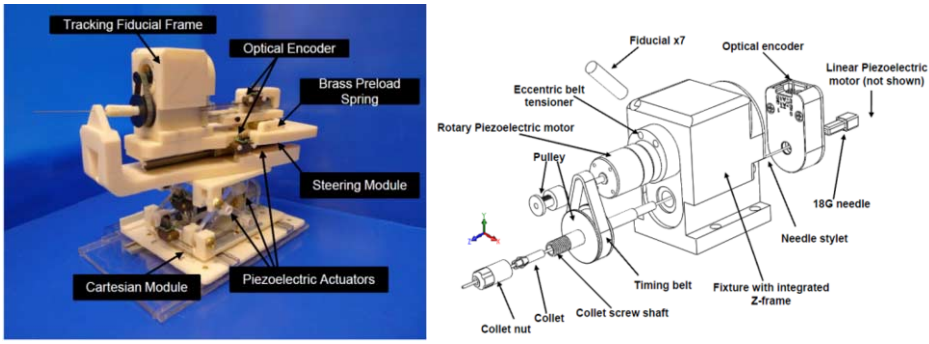

Figure 2: (Left) Physical prototype of 6-DOF piezoelectric needle placement robot consisting of needle driver module and Cartesian gross positioning module, (right) a exploded view of the needle clamping mechanism, optical tracking frame and rotary motor fixture with timing belt tensioner.

Once a preloaded needle or biopsy gun is inserted, the collet can rigidly clamp the cannula shaft. Since the linear motor is collinear with the collet and shaft, we need to offset the shaft to manually load the needle. We designed a brass spring preloaded mechanism that provides lateral passive motion freedom. The operator can squeeze the mechanism and offset the top motor fixture then insert the loaded needle through plain bearing housing and finally lock with the needle clamping. This structure allows for easy, reliable and rapid loading and unloading of standard needles.

2.2. Needle Placement Robot Navigation

Dynamic global registration between the robot and scanner is achieved by passive tracking the fiducial frame in front of the robot as shown in Fig. 2 (right). The rigid structure of the fiducial frame is made of ABS and seven MR Spot fiducials (Beekley, Bristol, CT) are embedded in the frame to form a Z shape passive fiducial. Any arbitrary MR image slicing through all of the rods provides the full 6-DOF pose of the frame, and thus the robot, with respect to the scanner [7]. Thus, by locating the fiducial attached to the robot, the transformation between patient coordinates (where planning is performed) and the needle placement robot is known. To enhance the system reliability and robust, multiple slices of fiducial images are used to register robot position using principal component analysis method. The end effector location is then calculated from the kinematics based on the encoder positions.

2.3. Piezoelectric Actuator Driver

The piezoelectric actuators (PiezoMotor, Uppsala, Sweden) chosen are non-harmonic piezoelectric motor which have two advantages over a harmonic drive: the noise caused by the driving wave is much easier to suppress, and the motion produced by the motors is generally at a more desirable speed and torque. Even though piezoelectric motor does not generate magnetic field, commercial motor driver boards usually induce significant image artifact due to electrical noise according to the most recent result [15]. A new low noise driver was developed and its architecture is shown in Fig. 3 (left) and Fig. 3 (right) shows the board prototype. Waveform tables are stored in RAM and utilized by a synthesizer running on the FPGA to generate four independent control waveforms of

arbitrary phase and frequency. These control waveforms are then streamed out to the analog amplification stage at 25 mega samples per second.

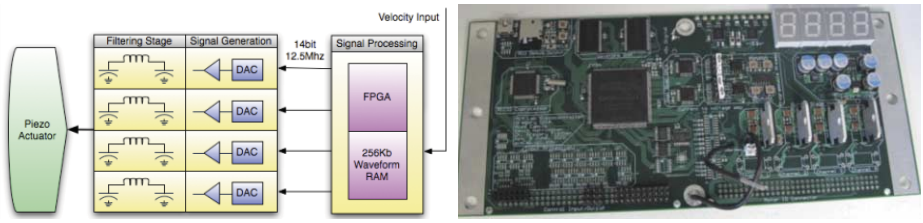

Figure 3: (Left) piezoelectric actuator driver architecture using FPGA generated waveform, (right) the piezoelectric driver board prototype, a key aspect of generating the low noise high precision motion.

3. Results

Four imaging protocols as shown in Table 1, were selected for evaluation of compatibility of the system: 1) diagnostic imaging T1-weighted fast gradient echo (T1 FGE/FFE), 2) diagnostic imaging T2-weighted fast spin echo (T2 FSE/TSE), 3) high-speed real-time imaging fast gradient echo (FGRE), and 4) functional imaging spin echo-planar imaging (SE EPI). Details of the scan protocols are shown in Table 1.

All sequences were acquired with a slice thickness of 5mm and a number of excitations (NEX) of one. Three configurations were evaluated and used in the comparison: 1) baseline of the phantom only, 2) motor powered with controllers DC power supply turned on and 3) system servoing inside MRI board. Three slices were acquired per imaging protocol for each configuration.

Table 1: SCAN PARAMETERS FOR COMPATIBILITY EVALUATION

Protocol	FOV	TE	TR	FA	Bandwidth
T1W FFE	240 mm	2.3 ms	225 ms	75°	751 Hz/pixel
T2W TSE	240 mm	90 ms	3000 ms	90°	158 Hz/pixel
FGRE	240 mm	2.1 ms	6.4 ms	50°	217 Hz/pixel
SE EPI	240 mm	45 ms	188 ms	90°	745 Hz/pixel

As can be seen in Fig. 4 (left), the motors and encoders provide very small visually identifiable interference with the operation of the scanner. Fig. 4 (right) depicts one slice of the tracking fiducial frame which provides the full position information of the robot. We utilize signal to noise ratio (SNR) as the metric for evaluating MR compatibility with baseline phantom image comparison. For comparison, the SNR of each configuration was normalized by the average SNR of the 3 baseline images for each imaging protocol. SNR was calculated as the mean signal in the center of the phantom divided by the noise intensity outside the phantom [10]. Statistical analysis with a Tukey Multiple Comparison confirms that no pair shows significant signal degradation with a *95%* confidence interval.

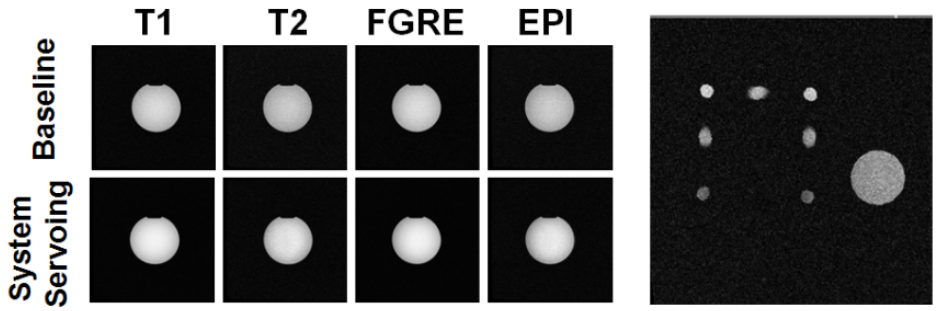

Figure 4: (Left) Representative results showing the images obtained of baseline and system servoing inside scanner bore conditions, (right) one slice of tracking fiducial frame besides a phantom. This result presents significant improvement over recent research [15].

4. Discussion

This paper presents the design of a MRI-compatible needle placement system actuated by piezoelectric actuators for transperineal prostate brachytherapy. It consists of a modular 3DOF needle driver module coupled with a 3-DOF *x-y-z* stage.

Initial comparability testing verified the system architecture and electrical comparability. This test has confirmed that no pair showed significant signal degradation with a *95%* confidence interval. Piezoelectric driven robot position control accuracy is being investigated. Future works include integrating the fiber optic sensors and phantom brachytherapy evaluation.

Acknowledgements

We gratefully acknowledge the support from the Congressionally Directed Medical Research Programs Prostate Cancer Research Program New Investigator Award W81XWH-09-1-0191 and Worcester Polytechnic Institute internal funds.

References

[1] A. Jemal, R. Siegel, E. Ward, Y. Hao, J. Xu, and M. J. Thun, “Cancer statistics, 2009,” CA Cancer J Clin, vol. 59, pp. caac.20006–249, May 2009.

[2] J. C. Presti, “Prostate cancer: assessment of risk using digital rectal examination, tumor grade, prostate-specific antigen, and systematic biopsy.” Radiol Clin North Am, vol. 38, pp. 49–58, Jan 2000.

[3] K. Chinzei and et al, "MR Compatible Surgical Assist Robot: System Integration and Preliminary Feasibility Study," in MICCAI 2000, 2000, pp. 921–930.

[4] A. Krieger, C. Csoma, I. I. Iordachital, P. Guion, A. K. Singh,G. Fichtinger, and L. L. Whitcomb, “Design and preliminary accuracy studies of an MRI-guided transrectal prostate intervention system.,” MICCAI2007, vol. 10, pp. 59–67, 2007.

[5] D. Stoianovici, D. Song, D. Petrisor, D. Ursu, D. Mazilu, M. Muntener, M. Mutener, M. Schar, and A. Patriciu, “MRI stealth robot for prostate interventions.,” Minim Invasive Ther Allied Technol, vol. 16, no. 4, pp. 241–248, 2007.

[6] S.E. Song, N. B. Cho, G. Fischer, N. Hata, C. Tempany, G. Fichtinger, and I. Iordachita, "Development of a pneumatic robot for MRI-guided transperineal prostate biopsy and brachytherapy: New approaches," in Proc. IEEE International Conference on Robotics and Automation ICRA, 2010.

[7] Fischer GS, Iordachita I, Csoma C, Tokuda J, DiMaio SP, Tempany CM, Hata N, Fichtinger G, MRI-Compatible Pneumatic Robot for Transperineal Prostate Needle Placement, IEEE / ASME Transactions on Mechatronics - Focused section on MRI Compatible Mechatronic Systems, Vol 13, No 3, pp 295-305, June 2008.

[8] Y. Wang, H. Su, K. Harrington and G. Fischer, "Sliding Mode Control of Piezoelectric Valve Regulated Pneumatic Actuator for MRI-Compatible Robotic Intervention", ASME Dynamic Systems and Control Conference, Boston, USA, 2010

[9] H. Su and G. S. Fischer, "High-field MRI-Compatible Needle Placement Robots for Prostate Interventions: Pneumatic and Piezoelectric Approaches", eds. T. Gulrez and A. Hassanien, Advances in Robotics and Virtual Reality, Springer-Verlag, to appear in 2011

[10] Y. Wang, G. Cole, H. Su, J. Pilitsis, and G. Fischer, "MRI compatibility evaluation of a piezoelectric actuator system for a neural interventional robot," in Annual Conference of IEEE Engineering in Medicine and Biology Society, (Minneapolis, MN), pp. 6072–6075, 2009.

[11] G. Cole, K. Harrington, H. Su, A. Camilo, J. Pilitsis, G. S. Fischer, "Closed-Loop Actuated Surgical System Utilizing In-Situ Real-Time MRI Guidance", 12th International Symposium on Experimental Robotics (ISER2010), New Delhi & Agra, India, 2010

[12] M. Mahvash and P. Dupont, "Fast needle insertion to minimize tissue deformation and damage," in Proc. IEEE International Conference on Robotics and Automation ICRA 2009, pp. 3097 – 3102, 2009.

[13] H. Su and G. Fischer, "A 3-axis optical force/torque sensor for prostate needle placement in magnetic resonance imaging environments," 2nd Annual IEEE International Conference on Technologies for Practical Robot Applications, (Boston, MA, USA), pp. 5–9, IEEE, 2009.

[14] H. Su, W. Shang, G. Cole, K. Harrington, and F. S. Gregory, "Haptic system design for MRI-guided needle based prostate brachytherapy," IEEE Haptics Symposium 2010, (Boston, MA, USA).

[15] A. Krieger, I. Iordachita, S. Song, N. Cho, G. Fichtinger, and L. Whitcomb, "Development and Preliminary Evaluation of an Actuated MRI-Compatible Robotic Device for MRI-Guided Prostate Intervention," in Proc. of IEEE International Conference on Robotics and Automation (ICRA 2010)